한국정밀공학회지 제 36 권 제 12 호 pp. 1173-1181 December 2019 / 1173
J. Korean Soc. Precis. Eng., Vol. 36, No. 12, pp. 1173-1181 https://doi.org/10.7736/KSPE.2019.36.12.1173
ISSN 1225-9071 (Print) / 2287-8769 (Online)

# 차량운전조건에 따른 에너지 하베스팅 현가장치의 발전량 민감도 분석 및 최적설계

# Sensitivity Analysis and Optimum Design of Energy Harvesting Suspension System according to Vehicle Driving Conditions

김태동[1], 김지혜[1], 김진호[1,#]
Tae Dong Kim[1], Ji Hye Kim[1], and Jin Ho Kim[1,#]

1 영남대학교 기계공학과 (Department of Mechanical Engineering, Yeungnam University)
# Corresponding Author / E-mail: jinho@ynu.ac.kr, TEL: +82-53-810-2441
ORCID: 0000-0002-6371-2828

KEYWORDS: Electromagnetic simulation (전자기 해석), Energy harvesting (에너지 하베스팅), Linear generator (선형 발전기), Vehicle suspension (차량 현가장치), Optimal design (최적설계)

*In this study, the sensitivity of the power generation effect of the applied linear generator of the energy harvesting suspension system under various input conditions was analyzed. The energy-harvesting suspension generates electric energy through energy harvesting using the road surface vibration energy during driving. Before analyzing the power generation effect, we analyzed the structure of the eight-pole Outer PM (Permanent Magnet) linear generator model using the electromagnetic suspension system to design the efficient generator, PIANO (Process Integration and Design Optimization). The ANSYS MAXWELL program was used to perform electromagnetic simulations of a linear generator model installed inside an energy-harvesting suspension to determine the power generation of the linear generator under various input conditions. The sensitivity of each input variable was compared by comparing the power generation effect of the energy-harvesting suspension device according to road displacement, frequency, and vehicle speed. The sensitivity to the road surface frequency was 1.9451, the sensitivity to the road surface amplitude was 1.0502, and the sensitivity to the vehicle speed was 0.6258. It is confirmed that the maximum sensitivity to the road surface displacement was demonstrated.*

Manuscript received: April 23, 2019 / Revised: September 30, 2019 / Accepted: October 1, 2019

## 1. Introduction

Energy Harvesting is a technology that harvests small energy that is not wasted or used everyday and converts it into usable electrical energy. It is attracting attention as a source of renewable energy. Because it can acquire electrical energy directly from nature, it is an eco-friendly energy utilization technology that can maintain energy supply safety, security and sustainability and reduce environmental pollution.[1] As electronic devices become smaller, the place where the battery is located is gradually disappearing. These problems have recently emerged as a new solution to 'Energy Harvesting'. The enormous energy that surrounds them eventually turns into sound or heat and disappears to the air. This discarded energy can be collected well and the efficiency of electronic devices can be much higher. We have not collected the [mW] power, but there is a field that can be used, and energy harvesting will play a role in small, low power electronic devices.[2,3] With advances in nanotechnology, even the smallest amount of energy that was previously abandoned can be effectively harvested. There are many advantages but many disadvantages as well. The biggest drawback is that the output is not constant. When it is cloudy or rainy, solar cells can not be used. Energy harvesting

uses various physical phenomena. Body energy harvesting uses body temperature, static electricity, kinetic energy, etc., which are generated through the movement of the body.[4,5] Solar energy harvesting using sunlight,[6] vibrational energy harvesting for generating piezoelectric elements by applying vibration or pressure, and the like.[7-9] Energy harvesting is being actively carried out mainly in Europe and the United States, and application fields will be further expanded.[10-12] In this study, energy harvesting technology using vibration energy was used, and the vibration energy was collected by attaching a generator to the suspension system, so that it could perform the self-generation function by converting it into electrical energy. Other existing researchers are also in the process of studying the energy harvesting of the body.[13-15] Outer PM 8 pole 8 slot model was used and the power generation effect of the linear generator was compared with the change of the road surface amplitude, road surface frequency and vehicle speed. Through Carsim-simulink, we confirmed the power generation effect according to the vehicle speed. Model simulation and power generation simulation were conducted using MAXWELL, a commercial electromagnetic analysis program. The optimum design is performed because it is necessary to design the optimal design because it requires the maximum power generation amount and minimum magnetic force.

## 2. Outer PM 8 Slot 8 Pole Linear Generator

The suspension is composed of a shock absorber, a spring, a suspension arm, etc., and is positioned between the axle and the vehicle body or the frame, supports the weight of the vehicle from the road surface while driving the vehicle, and alleviates the vibration of the wheel. Suspension is a viscous hydraulic system that absorbs shocks and is constructed with springs to suppress and eliminate vibration.[16-18] In this study, the suspension system is designed to generate electric energy through energy harvesting by absorbing up - down vibration energy. As shown in Fig. 1, the energy harvesting suspension system has a structure that can generate electric energy with vibration energy while removing vibration energy from damper.

Fig. 2 shows the structure of the existing suspension system and harvesting suspension system.

The generator used in this paper is an outer 8 slot 8 pole generator as shown in Fig. 3 and consists of a radial magnet, an axial magnet, a core, a coil, and a shaft and a guide for linear motion. The 8 slot 8 pole structure has eight coils and eight magnets facing each other. The structure of the linear generator has an inner and outer generator structure. In this paper, the outer PM 8

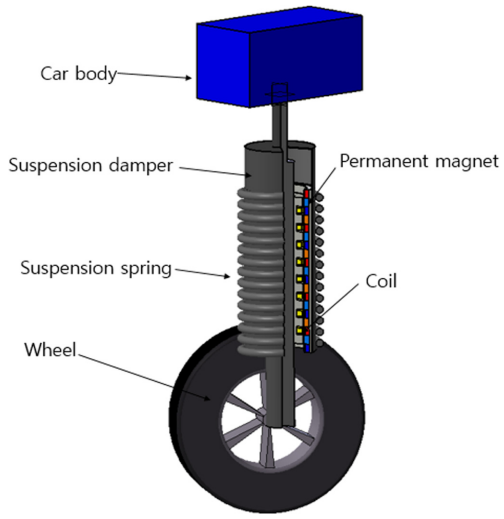


Fig. 1 Structure of regenerative suspension

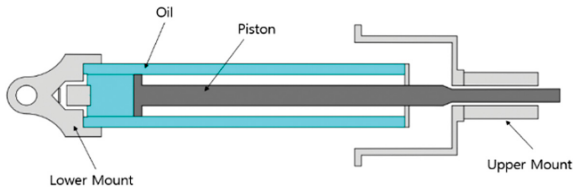


(a) Suspension

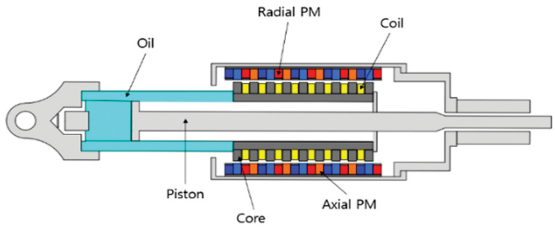


(b) Harvesting suspension

Fig. 2 Electromagnetic damper of vehicle suspension

slot 8 pole structure is selected to reduce the magnetic force. Simulation shows that the outer linear generator has relatively low magnetic force. Nd-Fe (Neodymium Ferrite) magnets with high magnetic force were used as magnets. The axial magnet is 40 SH and the radial magnet is 50 SH. In order to smooth the flow of magnetic force, the core is made of S20C material and arranged in order with the coil. It is an axisymmetric model and can be divided into a mover and a stator. The generation motion is established by the relative motion of the mover and the stator. The up and down motion of the mover with the permanent magnet passes over the coils of the stator, and the electromotive force (EMF) is induced in the coil to generate electric energy. Can be expressed by the following Eq. (1).

$$e(t) = N\frac{d\phi dz}{dz\,dt} \tag{1}$$

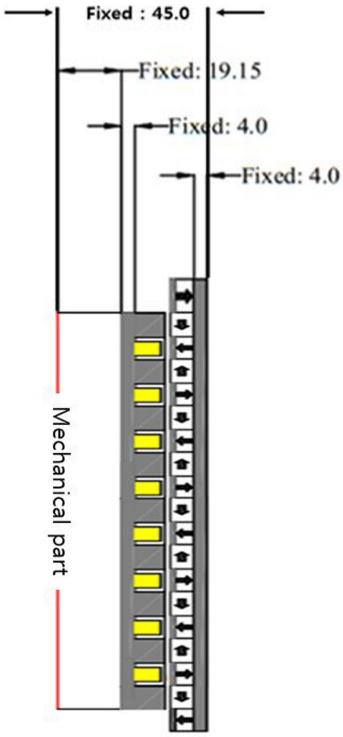


Fig. 3 8 Slot 8 Pole 1/4 model

Where $N$ is the number of turns of the coil, phi is the flux passing through each turn for a time $t$, and $dz/dt$ is the velocity for the $z$ direction displacement of the mover.

## 3. Optimal Design

### 3.1 Design Variables and Constraints

In this paper, the optimum design is achieved by adjusting various parameters for maximum power generation and minimum axial force. This is because the power generation and the axial force produce different results depending on the sizes and positions of the magnets, coils, and cores of the generator. To design the optimal design, four design variables were selected. Tooth thickness, tooth width, spacer thickness, and axial PM width were selected as shown in Fig. 4. Other parameters that are not selected are determined by the constraints, which are 38.3 mm inside diameter, 90 mm outside diameter, 23 mm pole pitch, and 1 mm for air gap. The thickness of the inner and outer cores is fixed at 4 mm. The radial PM width is determined by the pole pitch and the axial PM width, and the radial PM thickness is determined by the axial PM thickness and the spacer thickness. As shown in Figs. 4(b) and 4(c), other variables are determined by the location conditions. The size and position of the coil are determined by the size of the left and right cores. Table 1 shows the range of design variables.

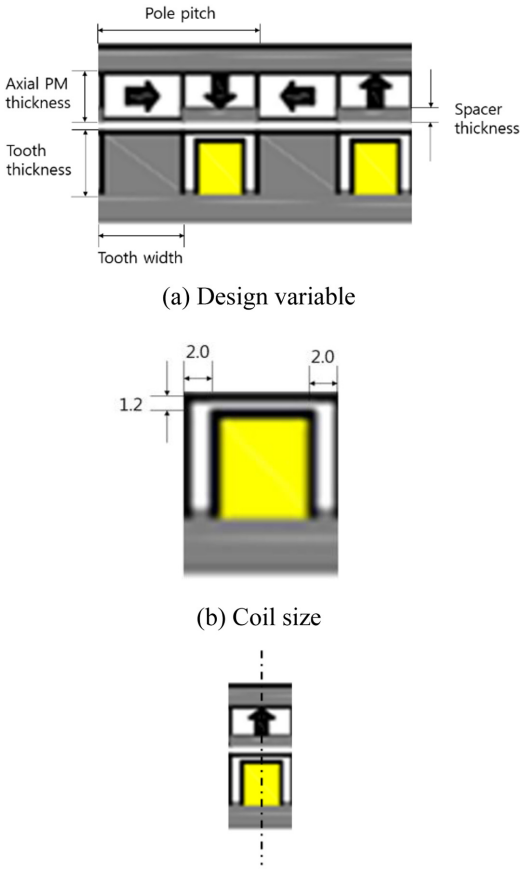


Fig. 4 Design variables of optimal design

Table 1 Boundary condition of optimal design variables

| | Low | High |
|---|---|---|
| Tooth thickness [mm] | 6.0 | 10.0 |
| Tooth width [mm] | 6.0 | 12.0 |
| Spacer thickness [mm] | 1.5 | 3.5 |
| Axial PM width [mm] | 6.0 | 12.0 |

The optimum design results are the maximum power generation, the average power generation, and the minimum axial force.

### 3.2 Design of Experiment

For the maximum average power generation, the number of design variables was considered using the orthogonal array table provided by PIANO (Process Integration, Automation and Optimization), a commercial PIDO (Process Integration and Design Optimization) tool. 36 experimental points were obtained and power generation amount and axial force were calculated using commercial electromagnetic analysis program ANSYS MAXWELL. The finite element analysis was performed at the speed indicated in Eq. (2).

Table 2 Result of optimization

| | Initial | Optimal |
|---|---|---|
| Tooth thickness [mm] | 9.000 | 9.938 |
| Tooth Width [mm] | 12.000 | 9.003 |
| Spacer Thickness [mm] | 1.500 | 2.386 |
| Axial PM width [mm] | 12.000 | 6.000 |

Table 3 Simulation result of optimal design

| | Result | | Analysis |
|---|---|---|---|
| | Optimal | Simulation | Error ratio [%] |
| Maximum power [W] | 272.9 | 278.4 | 2.0 |
| Average Power [W] | 79.13 | 82.13 | 3.79 |
| Max force [kN] | 1.713 | 1.790 | 4.495 |

$$s = A \times \sin 2\pi ft$$
$$v = ds/dt = A \times 2\pi f \times \cos 2\pi ft \quad (2)$$
$$v = 5.625 \times 2\pi \times 10 \times \cos 2\pi \times 10 \times \text{time}$$

The stop time was set to 0.3 s and the time step was set to 0.001 s. The initial frequency $f$ was advanced to 10 Hz, which is the average frequency of the road surface. The reason that the stop time is performed with a small time of 0.3 s is because the equation related to the speed is derived as a cosine form and the same result is obtained even if a lot of time is elapsed.

### 3.3 Approximation Model

A Kriging model was created among various approximate models. A representative interpolation model, Kriging, is a statistical technique that predicts the known values in a linear combination with good predictive performance in nonlinear systems with many design variables.[19] We generated the Kriging model using the approximation method provided by the PIANO program through the simulation results of 36 experimental point.

### 3.4 Evolutionary Algorithm

The optimal design using the approximated Evolutionary Algorithm was performed. The evolutionary algorithm generates the next population by generating random variables within a certain range from the parent population, which is a design variable set as one of the probabilistic optimization techniques.[20] The design variables are reconstructed by selecting the variables closest to the desired design goal through the parent population and the next population. The accuracy of the Kriging model was verified by the approximation method and the generator model was created

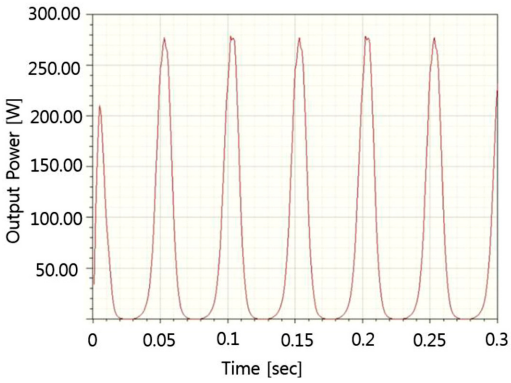


(a) Output power graph

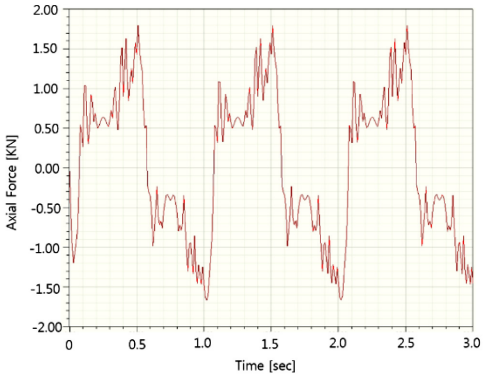


(b) Axial force graph

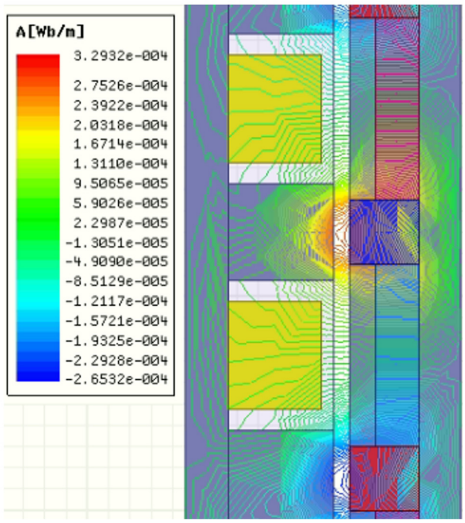


(c) Flux line of electromagnetic simulation

Fig. 5 Optimal model simulation result

using the variable values shown in Table 2 through the evolution algorithm. Table 2 also shows the dimensions for the initial model.

### 3.5 Verification of Design Result

For the accuracy of the optimum design result, the generated power and the axial force are calculated by electromagnetic simulation using the derived design variables, and errors within 5% are shown in Table 3.

Table 4 Amplitude data

| Amplitude [mm] | Maximum power [W] | Average Power [W] | Max force [kN] |
|---|---|---|---|
| 2.8125 | 78.3088 | 29.5449 | 1.5099 |
| 3.3750 | 109.8014 | 38.3326 | 1.5985 |
| 3.9375 | 147.9391 | 46.7228 | 1.6160 |
| 4.5000 | 187.7107 | 54.8055 | 1.6913 |
| 5.0625 | 229.1063 | 62.5779 | 1.7659 |
| 5.6250 | 278.4210 | 70.1057 | 1.7896 |
| 6.1875 | 334.0051 | 77.2733 | 1.8070 |
| 6.7500 | 392.4361 | 84.1492 | 1.8491 |
| 7.3125 | 452.1469 | 90.8397 | 1.9619 |
| 7.8750 | 513.9067 | 97.2975 | 2.1116 |
| 8.4375 | 584.5853 | 103.5934 | 2.2354 |

In comparison with the initial model, the maximum power generation amount increased by 59.98%, the average power generation amount increased by 78.68%, and the magnetic force decreased by 66.31%. The power generation, magnetic force, and flux diagram of the optimal model are shown in Fig. 5.

## 4. Generator Simulation Based on Vehicle Driving Conditions

### 4.1 Simulation of Generators according to Road Surface Displacement

Generator was created based on extracted data through optimal design. Simulation of the generator was carried out using the road surface displacement as a variable. Based on the existing displacement of 5.625 mm, 10 road surface displacements were extracted by increasing and decreasing by 10%. The total analysis time was set to 5 s and the time step was set to 0.001 s. 11 data were processed in the same way, and the surface displacement, amplitude, maximum power generation, average power generation and magnetic force are shown in Table 4. The velocity shown in Eq. (3) was used and the frequency was 10 Hz.

$$v = \frac{ds}{dt} = A \times 2\pi f \times \cos 2\pi f t \tag{3}$$

As the road surface displacement increased, the maximum power generation and average power generation also increased significantly. The magnetic force also increased. Fig. 6 shows the velocity graph in the case of at $A$ = 2.8125 mm, 5.625 mm, and 8.4375 mm.

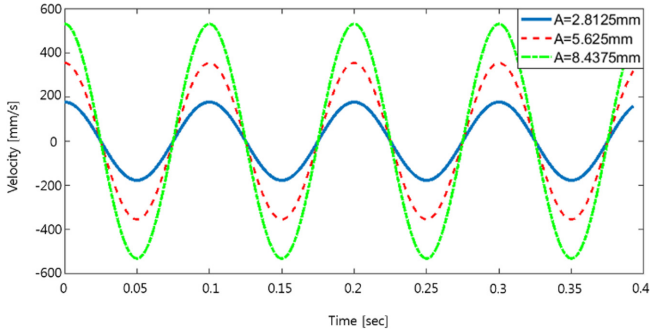


Fig. 6 Velocity graph of amplitude

Table 5 Frequency data

| Frequency [Hz] | Maximum power [W] | Average power [W] | Max force [kN] |
|---|---|---|---|
| 5 | 80.1091 | 18.2548 | 1.6125 |
| 6 | 112.4830 | 26.2674 | 1.6447 |
| 7 | 149.0175 | 38.6514 | 1.6426 |
| 8 | 188.8233 | 44.3883 | 1.7031 |
| 9 | 232.3786 | 60.3373 | 1.7468 |
| 10 | 278.4210 | 70.1057 | 1.7896 |
| 11 | 332.1321 | 85.6672 | 2.0960 |
| 12 | 388.6620 | 105.7173 | 2.2113 |
| 13 | 446.2688 | 115.0291 | 2.3263 |
| 14 | 510.8456 | 138.9770 | 2.2257 |
| 15 | 574.6269 | 151.9005 | 2.3809 |

### 4.2 Simulation of Generators according to Frequency

Simulation of the generator was performed according to the change in frequency. The existing road surface frequency was 5.625 mm. 10 frequencies were extracted in the same manner. The analysis was conducted under the same conditions as before. Each frequency, power generation and magnetic force are shown in Table 5.

As the frequency increased, the power generation increased significantly. The magnetic force seemed to increase largely, but the magnetic force was increased and the data decreased in frequency larger than the reference frequency. The velocity graph at $f$ = 5 Hz, 10 Hz, and 15 Hz is shown in Fig. 7.

### 4.3 Simulation of Generators according to Vehicle Velocity

As the vehicle velocity changed, the generator simulation was performed. The velocity of the suspension according to the vehicle speed was extracted by using Carsim-simulink. Carsim is software that simulates passenger cars and light trucks and allows analysis of the response of various vehicles. Simulink in MATLAB is a model-based design tool built from a block diagram of the system,

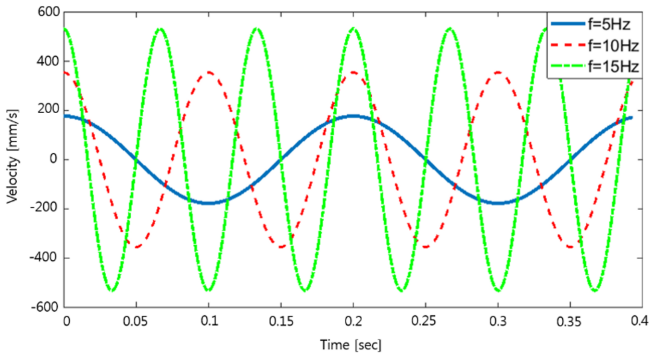


Fig. 7 Velocity graph of frequency

Fig. 8 Vehicle model

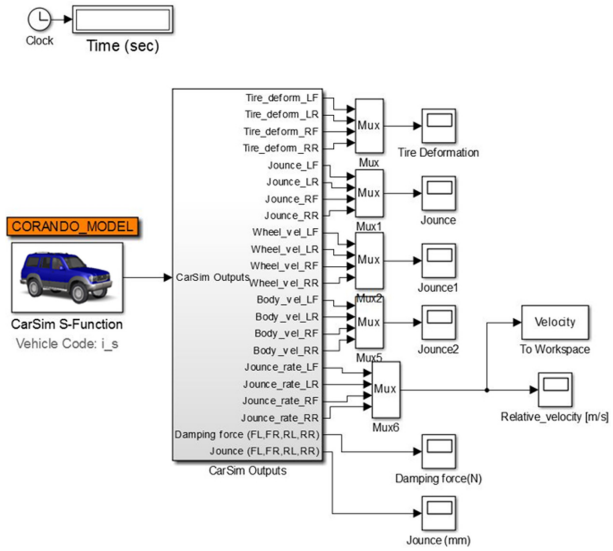


Fig. 9 Block diagram

and many simulations and vehicle studies have been conducted with Carsim, such as running simulations and vehicle dynamics simulations. In 2018, a cruise control system based on fuzzy PID control has been studied to assist the driver in driving.[21] Vehicle model is shown in Fig. 8, and the main characteristic of the vehicle are shown in Table 6.

Fig. 9 is a block diagram of the vehicle system used in this study.

Fig. 10 shows the road roughness and the velocity of the suspension according to the velocity of the vehicle is derived.

The speed of the suspension is shown in Fig. 11, and the

Table 6 Vehicle model characteristics

| | |
|---|---|
| Sprung mass | 2257 kg |
| Unsprung mass | 100 kg |
| Front wheel – Rear wheel | 2946 mm |
| Internal engine model | 250 kw |
| Velocity of vehicle | 30 km/h |

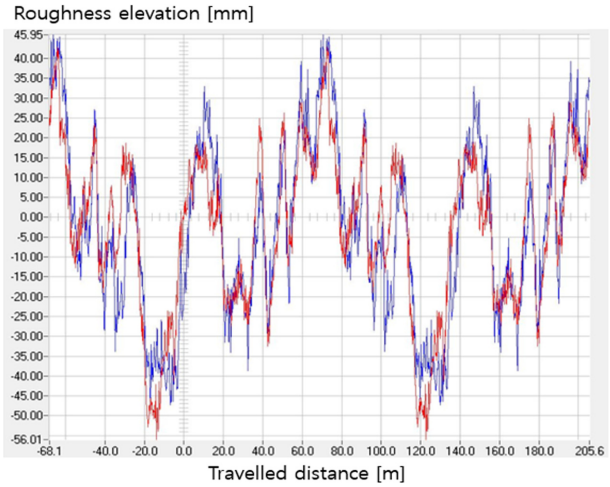


Fig. 10 Road roughness

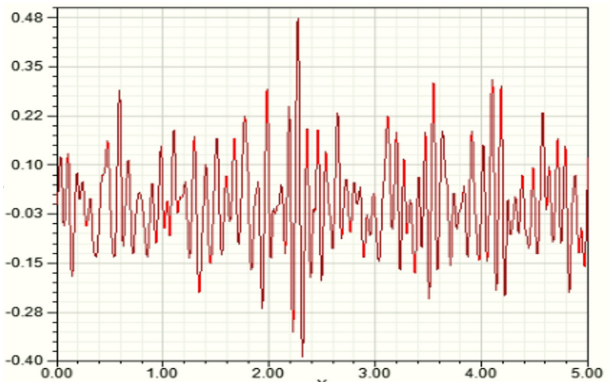

Fig. 11 Speed of the suspension

MAXWELL simulation was performed by setting the total analysis time to 5 s and the time step to 0.001 s. Table 7 shows the generated power and magnetic force.

## 5. Sensitivity Analysis of Power Generation according to Driving Conditions

In this study, the power generation and magnetic force were observed according to the driving conditions of the vehicle. Sensitivity analysis was conducted to find out which conditions are most sensitive to each condition. The ratio of the rate of change of

Table 7 Vehicle velocity data

| Vehicle velocity [km/h] | Maximum power [W] | Average power [W] | Max force [kN] |
|---|---|---|---|
| 20 | 122.2651 | 8.7903 | 1.6534 |
| 22 | 193.3701 | 9.7585 | 1.7067 |
| 24 | 282.0634 | 11.1354 | 1.7218 |
| 26 | 358.3982 | 12.5170 | 1.9030 |
| 28 | 403.6553 | 13.6208 | 1.9022 |
| 30 | 426.8277 | 14.2737 | 1.7918 |
| 32 | 455.1234 | 14.5312 | 1.6709 |
| 34 | 487.2917 | 15.0704 | 1.8625 |
| 36 | 448.9052 | 15.0679 | 1.9046 |
| 38 | 346.4972 | 14.7332 | 1.7129 |
| 40 | 707.5874 | 14.8905 | 1.7366 |

the average power generation to the rate of change of design variables is shown expressed in Eq. (4).

$$S = \frac{\frac{\Delta W}{W_{initial}}}{\frac{\Delta X}{X_{initial}}} \tag{4}$$

In Eq. (4), $S$ represents the sensitivity, $\Delta X/X_{initial}$ in the denominator represents the rate of change with respect to the initial value of the design variable, and $\Delta W/W_{initial}$ in the numerator represents the rate of change of the corresponding generation amount. The initial condition is $f$ = 10 Hz, $A$ = 5.625 mm, $v_{vehicle\ velocity}$ = 30 km/h. The average sensitivity for road surface frequency, amplitude, and vehicle speed is shown in Fig. 12 as a graph.

Sensitivity to each condition was determined. The average sensitivity for each variable was 1.9451 for road surface, 1.0502 for amplitude, and 0.6258 for vehicle speed. It was confirmed that the road surface amplitude and the vehicle speed do not show a large sensitivity relative to the road surface frequency.

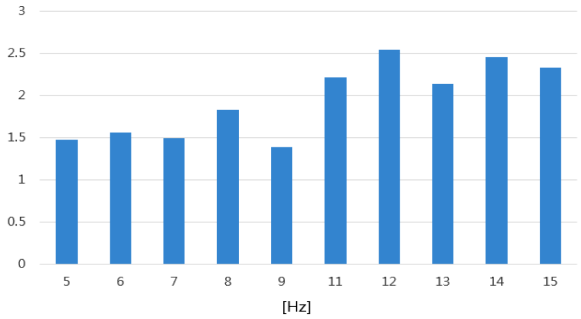


(a) Road frequency [Hz]

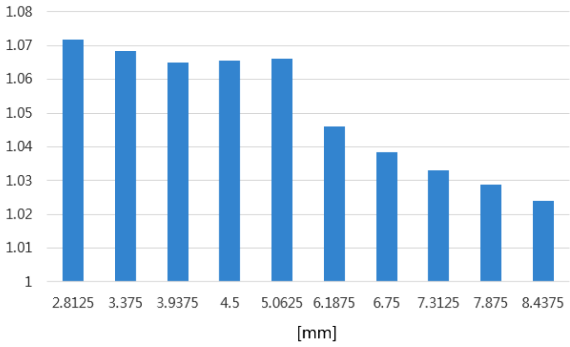


(b) Amplitude [mm]

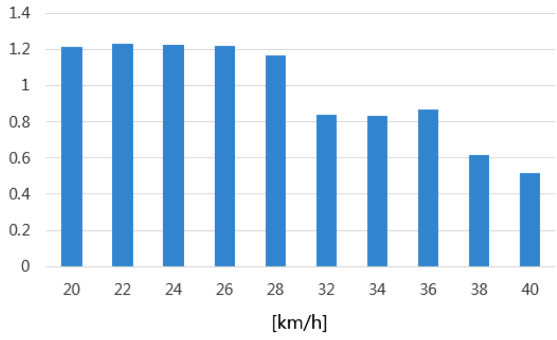


(c) Vehicle velocity [km/h]

Fig. 12 Sensitivity to average power

## 6. Conclusions

In this study, the verification of the power generation of the harvesting suspension system was carried out. In order to derive the optimal model with maximum power generation and minimum magnetic force, the optimal design was performed by using PIANO, a PIDO tool, with four parameters. Next, the optimal model of the linear generator was verified by using electromagnetic simulation ANSYS MAXWELL. In the initial model, the maximum power generation amount was 174.0479 W, the average power generation amount was 45.9855 W, the maximum magnetic power was 2.7002 kN, and the maximum model generation amount was 278.4210 W, the average generation amount was 70.1067 W and the maximum magnetic power was 1.7896 kN. The maximum power generation amount was 59.98%, the average power generation amount was 78.68% higher than the initial model, and the optimum power generation amount with magnetic force decreased by 66.31% was derived. Lastly, three input conditions were applied to analyze the sensitivity of power generation according to changes in road surface displacement, road surface frequency, and vehicle velocity. Suspension velocity according to vehicle velocity was derived through a simulated driving test using the Carsim-simulink. We observed that the average power generation is the most sensitive to the road surface

frequency. Sensitivity to road surface frequency is 1.9451, sensitivity to road surface displacement is 1.0502, sensitivity to vehicle speed is 0.6258.

## REFERENCES


1. Beeby, S. P., Torah, R., Tudor, M., Glynne-Jones, P., O'donnell, T., et al., "A Micro Electromagnetic Generator for Vibration Energy Harvesting," Journal of Micromechanics and Microengineering, Vol. 17, No. 7, pp. 1257-1265, 2007.
2. Manla, G., White, N., and Tudor, J., "Harvesting Energy from Vehicle Wheels. Solid-State Sensors, Actuators and Microsystems," Proc. of the International Solid-State Sensors, Actuators and Microsystems Conference, pp. 1389-1392, 2009.
3. Wischke, M., Masur, M., and Woias, P., "A Hybrid Generator for Virbration Energy Harvesting Applications," Proc. of the International Solid-State Sensors, Actuators and Microsystems Conference, pp. 521-524, 2009.
4. Mateu, L., Codrea, C., Lucas, N., Pollak, M., and Spies, P., "Human Body Energy Harvesting Thermogenerator for Sensing Applications," Proc. of the International Conference on Sensor Technologies and Applications, pp. 366-372, 2007.
5. Mitcheson, P. D., Yeatman, E. M., Rao, G. K., Holmes, A. S., and Green, T. C., "Energy Harvesting from Human and Machine Motion for Wireless Electronic Devices," Proc. of the IEEE, Vol. 96, No. 9, pp. 1457-1486, 2008.
6. López-Lapeña, O., Penella, M. T., and Gasulla, M., "A New MPPT Method for Low-Power Solar Energy Harvesting," IEEE Transactions on Industrial Electronics, Vol. 57, No. 9, pp. 3129-3138, 2009.
7. Wei, C. and Jing, X., "A Comprehensive Review on Vibration Energy Harvesting: Modelling and Realization," Renewable and Sustainable Energy Reviews, Vol. 74, pp. 1-18, 2017.
8. Lei, Z. and Xiudong, T., "Large-Scale Vibration Energy Harvesting," Journal of Intelligent Material Systems and Structures, Vol. 24, No. 11, pp. 1405-1430, 2013.
9. Abdelkareem, M. A., Xu, L., Ali, M. K. A., Elagouz, A., Mi, J., et al., "Vibration Energy Harvesting in Automotive Suspension System: A Detailed Review," Applied Energy, Vol. 229, pp. 672-699, 2018.
10. Challa, V. R., Prasad, M., Shi, Y., and Fisher, F. T., "A Vibration Energy Harvesting Device with Bidirectional Resonance Frequency Tunability," Smart Materials and Structures, Vol. 17, No. 1, Paper No. 015035, 2008.
11. Starner, T. and Paradiso, J. A., "Human Generated Power for Mobile Electronics," Low-Power Electronics Design, Vol. 45, pp. 1-35, 2004.
12. Polinder, H., Mueller, M., Scuotto, M., and Goden de Sousa Prado, M., "Linear Generator Systems for Wave Energy Conversion," Proc. of the 7th European Wave and Tidal Energy Conference, 2007.
13. Li, Z., Zuo, L., Kuang, J., and Luhrs, G., "Energy-Harvesting Shock Absorber with a Mechanical Motion Rectifier," Smart Materials and Structures, Vol. 22, No. 2, Paper No. 025008, 2012.
14. Asadi, E., Ribeiro, R., Khamesee, M. B., and Khajepour, A., "A New Adaptive Hybrid Electromagnetic Damper: Modelling, Optimization, and Experiment," Smart Materials and Structures, Vol. 24, No. 7, Paper No. 075003, 2015.
15. Martins, I., Esteves, J., Marques, G. D., and Da Silva, F. P., "Permanent-Magnets Linear Actuators Applicability in Automobile Active Suspensions," IEEE Transactions on Vehicular Technology, Vol. 55, No. 1, pp. 86-94, 2006.
16. Hrovat, D., "Survey of Advanced Suspension Developments and Related Optimal Control Applications," Automatica, Vol. 33, No. 10, pp. 1781-1817, 1997.
17. Abdelkareem, M. A., Makrahy, M. M., Abd-El-Tawwab, A. M., EL-Razaz, A., Kamal Ahmed Ali, M., et al., "An Analytical Study of the Performance Indices of Articulated Truck Semi-Trailer During Three Different Cases to Improve the Driver Comfort," Journal of Multi-Body Dynamics, Vol. 232, No. 1, pp. 84-102, 2018.
18. Karnopp, D., "Active and Semi-Active Vibration Isolation," Journal of Vibration and Acoustics, Vol. 117, pp. 177-185, 1995.
19. Kim, J. K. and Lee, K. H., "A Structural Design of Microgyroscope Using Kriging Approximation Model," Journal of the Korean Society of Manufacturing Process Engineers, Vol. 7, No. 4, pp. 149-154, 2008.
20. Jang, J. H. and Kim, J. H., "Optimal Design for Improved Rotation Latch System Performance," Journal of the Korean Society of Manufacturing Process Engineers, Vol. 14, No. 5, pp. 102-106, 2015.
21. Zhao, S. and Zhu, L., "Cruise Control System based on Joint Simulation of CarSim and Simulink," Open Access Library Journal, Vol. 5, No. 7, pp. 1-8, 2018.


**Tae Dong Kim**
Master candidate in the Department of Mechanical Engineering, Yeungnam University. His research interest is design of Ultra precision motor and actuators..
E-mail: rlaxoehd3311@ynu.ac.kr

**Ji Hye Kim**
Master candidate in the Department of Mechanical Engineering, Yeungnam University. His research interest is design of Ultra precision motor and actuators. E-mail: jihye2204@ynu.ac.kr

**Jin Ho Kim**
Ph.D. in the Department of Mechanical Engineering, U.C. Berkeley. He is a professor at Yeungnam University. His research interest is design of Ultra precision motor and actuators.
E-mail: jinho@ynu.ac.kr